Available online at www.sciencedirect.com
ScienceDirect
Journal of Power Sources 170 (2007) 465–475
JOURNAL OF POWER SOURCES
www.elsevier.com/locate/jpowsour

Performance degradation of high-power lithium-ion cells—Electrochemistry of harvested electrodes

D.P. Abraham [a,*], J.L. Knuth [a], D.W. Dees [a], I. Bloom [a], J.P. Christophersen [b]

[a] *Argonne National Laboratory, Argonne, IL 60439, USA*
[b] *Idaho National Laboratory, Idaho Falls, ID 83415, USA*

Received 15 February 2007; received in revised form 20 March 2007; accepted 29 March 2007
Available online 18 April 2007

Abstract

The performance of 18650-type high-power lithium-ion cells is being evaluated as part of the U.S. Department of Energy's (DOEs) Advanced Technology Development (ATD) program. In this article, we present accelerated aging data acquired on 18650-cells containing $LiNi_{0.8}Co_{0.15}Al_{0.05}O_2$- or $LiNi_{0.8}Co_{0.1}Al_{0.1}O_2$-based positive electrodes, MAG-10 graphite-based negative electrodes, and 1.2-M $LiPF_6$ in EC:EMC (3:7 by wt.) electrolyte. Capacity and impedance data acquired on electrodes harvested from these cells highlight the contributions of the positive and negative electrodes to the degradation of cell performance. We also describe test methodologies used to examine the electrochemical characteristics of the harvested electrodes. Identifying and optimizing cell components responsible for performance degradation should enable the development of new lithium-ion cell chemistries that will meet the 15-year cell calendar life goal established by DOEs FreedomCar initiative. Published by Elsevier B.V.

Keywords: High-power; Lithium-ion; Impedance rise; Capacity fade

1. Introduction

Lithium-ion batteries currently power millions of portable electronic devices worldwide. These cells have high energy density, excellent cycle life, wide operating temperature range, and long shelf life. Because of their relatively high-power densities, lithium-ion cells are also attractive as energy storage devices for hybrid electric vehicles (HEVs) [1]. These devices deliver and accept high-power pulses during vehicle acceleration (rapid discharge capability) and braking (rapid charging capability), respectively. Because cell discharging and charging involves lithium-ion diffusion within the electrolyte, through the electrolyte–electrode interface and the electrode, any resistance to charge movement contributes to the internal impedance of the cell. Consequently, an increase in impedance degrades the power performance of the cell [2–6].

The performance of 18650-type lithium-ion cells (18 mm dia., 65 mm long) specifically designed for high-power applications is being evaluated as part of the U.S. Department of Energy's (DOEs) Advanced Technology Development (ATD) program [7–10]. These cells are tested under various accelerated aging conditions to determine calendar-life and cycle-life performance. Changes during cell testing are determined by C_1/1 and C_1/25 capacity measurements and hybrid pulse power characterization (HPPC) and electrochemical impedance spectroscopy (EIS) measurements. The resulting data indicate that capacity fade and impedance rise are determined by several factors, including aging temperature, cell voltage (i.e., state-of-charge, SOC), cycling parameters, and electrode material composition. All cell groups studied to date reach end-of-life because of increasing impedance and corresponding power loss. Deriving performance degradation mechanisms from the 18650-cell test results is difficult because the measured data represent a superposition of several processes occurring in the cell.

In this article, we describe representative accelerated aging data acquired over a 4-year period on 18650-cells containing $LiNi_{0.8}Co_{0.15}Al_{0.05}O_2$- or $LiNi_{0.8}Co_{0.1}Al_{0.1}O_2$-based positive electrodes, MAG-10 graphite-based negative electrodes, and a 1.2-M $LiPF_6$ in ethylene carbonate: ethyl methyl carbonate (EC:EMC) (3:7 by wt.) electrolyte (henceforth referred to as Gen2 electrolyte). Electrochemical experiments conducted on electrodes harvested from these 18650-cells highlight contribu-

* Corresponding author. Tel.: +1 630 252 4332; fax: +1 630 972 4406.
E-mail address: abraham@cmt.anl.gov (D.P. Abraham).

0378-7753/$ – see front matter. Published by Elsevier B.V.
doi:10.1016/j.jpowsour.2007.03.071

tions of the positive and negative electrodes to cell capacity and impedance rise. We describe test methodologies used to examine the electrochemical characteristics of the harvested electrodes. Data from the spectroscopy, microscopy, and diffraction studies on components from these 18650-cells, and mechanisms responsible for cell performance degradation, will be detailed in a separate article.

2. Experimental procedure

The cells were of the standard 18650-size, however they were custom designed for high-power performance and for better hermeticity. The cells employed 10 tabs along the length of both the positive and negative electrodes to reduce the resistance associated with the current collection system during high-current charge and discharge pulses. Also, the cells employed an aluminum case, which was connected to the positive electrode, and the cells were sealed by a laser weld. All cells were leak checked, to ensure a high degree of hermeticity, prior to being shipped. Table 1 lists details of electrode construction and cell chemistry.

The cells containing $LiNi_{0.8}Co_{0.15}Al_{0.05}O_2$-based positive electrodes (Gen2 cells) had a starting C_1/1 capacity of about one ampere-hour (∼1 Ah); the cells containing $LiNi_{0.8}Co_{0.1}Al_{0.1}O_2$-based positive electrodes (VarC cells) had a starting C_1/1 capacity of ∼0.8 Ah. The positive electrode oxide composition was the only difference between the Gen2 and VarC cells; the level of Al dopant was increased from 5% (Gen2) to 10% (VarC) to improve the oxide's stability.

After formation cycling by the manufacturer, Quallion, LLC, the cells were shipped to Argonne National Laboratory (ANL) or Idaho National Laboratory (INL) for performance testing and accelerated aging. Initial performance tests on the cells included (1) electrochemical cycling between 3 and 4.1 V to determine 1 h (C_1/1) and 25 h (C_1/25) capacities, (2) HPPC tests to determine cell impedance and dynamic power capability under high current (∼5C rate) discharge- and charge-pulses, and (3) EIS at 3.72 V (∼60% SOC) to determine cell impedance over a range of applied frequencies. The cells were then subjected to calendar- and cycle-life aging according to standard test protocols [11]. The aging was conducted at 25, 45, and 55 °C. The "calendar-life" cells were nominally held at 3.72 V during aging. The "cycle-life" cells were subjected to shallow cycling, ∼1200 cycles a day, at about 3.72 V. Every 4 weeks, the cells were cooled to 25 °C and tested to determine changes in capacity and impedance. Details of the test protocol and a summary of the test data are available in Ref. [7]. Throughout the aging process, selected cells were removed at predetermined intervals for detailed diagnostic evaluation.

The 18650-cells were discharged to 3.1 V (0% state-of-charge) before disassembly in an Ar-atmosphere glove box (<1 ppm H_2O, <5 ppm O_2). Electrochemical tests were conducted on the harvested electrodes to determine the effect of aging on electrode performance. The coating on one side of the double-sided electrode laminate had to be removed before electrochemical measurements were conducted because experiments with double-sided electrodes showed unacceptably rapid voltage loss with time, apparently from current leaks at the electrode edges. The coating-removal was conducted gently to minimize material damage. The electrode was placed on a glass mirror and lightly dabbed with 1-methyl-2-pyrolidinone solvent to dissolve the PVdF binder. Dabbing was repeated until the coating peeled off the current collector foil when rubbed with a cotton-based wipe. Precautions were taken to avoid solvent seepage to the other side (i.e., the side on which the electrochemical measurements were made). To obtain reliable and reproducible data, the coating-removal was conducted in an Ar- or He-atmosphere glovebox. Erratic data were often obtained from electrodes that were stripped in a dry-room or in a N_2-atmosphere glove box.

Electrochemical data were obtained on electrodes harvested from more than 30 cells aged under various conditions and showing a range of capacity and power loss. In this article, for brevity, we report data from selected cells that represent the observed impedance and capacity trends (see Table 2). Reference electrode cells were prepared to determine the relative contributions of the positive and negative electrodes to impedance rise. The reference electrode cells were assembled with 15.5 cm^2 electrodes, two Celgard 2325 separators enveloping a Li–Sn reference electrode, and fresh Gen2 electrolyte.

Table 1
Gen2/VarC cell chemistry (average electrode area = 846.3 cm^2)

Positive electrode	Negative electrode
84 wt.% $LiNi_{0.8}Co_{0.15}Al_{0.05}O_2$ (Fuji CA1505) or 84 wt.% $LiNi_{0.8}Co_{0.1}Al_{0.1}O_2$	92 wt.% MAG-10 graphite (Hitachi)
8 wt.% PVdF binder (Kureha KF-1100)	8 wt.% PVdF binder (Kureha #C)
4 wt.% SFG-6 graphite (Timical)	
4 wt.% carbon black (Chevron)	
8 mg cm^{-2} loading density	4.9 mg cm^{-2} loading density
35 μm-thick coating/side	35 μm-thick coating/side
30 μm-thick Al current collector	18 μm-thick Cu current collector
Electrolyte	**Separator**
1.2-M $LiPF_6$ in EC:EMC (3:7 by wt.)	25 μm thick (Celgard 2300)

Table 2
Aging conditions, C_1/1 capacity fade (CF) data, and area specific impedance (ASI) increase data for 18650-cells from which electrodes were harvested for electrochemical analysis

Cell type	Aging *T*, period, type	CF (%)	ASI rise (%)
Gen2	0 week	0	0
Gen2	55 °C, 4 weeks, calendar	3.7	11.7
Gen2	55 °C, 32 weeks, calendar	14	31.3
Gen2	55 °C, 40 weeks, calendar	18.3	43.4
Gen2	45 °C, 88 weeks, calendar	34.4	90.1
Gen2	45 °C, 32 weeks, cycle	10	25.2
Gen2	45 °C, 68 weeks, cycle	30	77.2
Gen2	25 °C, 136 weeks, cycle	34.1	87.5
VarC	0 week	0	0
VarC	45 °C, 4 weeks, cycle	1.8	10.8
VarC	45 °C, 40 weeks, cycle	3.8	18.8
VarC	45 °C, 40 weeks, calendar	1.8	39.1
VarC	45 °C, 60 weeks, calendar	2.7	84.2

Details on the Li–Sn micro-reference electrode, cell assembly, test equipment, and test procedures are discussed elsewhere (see Ref. [12]).

Coin cells (2032-type) were assembled with 1.6 cm^2-area samples punched from the harvested electrodes, lithium-metal counter electrode, fresh Celgard 2325 separator, and fresh Gen2 electrolyte to determine the effect of aging on electrode capacity. The cells containing the positive electrode (cathode) were cycled from 3 to 4.3 V, and the cells containing the negative electrode (anode) were cycled from 0 to 1.5 V. The cycling was conducted at various current densities (~C_1/5 to C_1/200) to determine the effect of the cycling rate on cell capacity. Data were obtained both at room temperature and at 55 °C for some electrodes. The effect of rinsing on electrode performance was also examined.

Although we took precautions to minimize testing artifacts during material preparation and cell assembly, it should be noted that all measurements obtained with harvested electrode cells have an inherent uncertainty, associated with the 18650-cell disassembly process. In addition, the electrode stack pressure, gas environment, electrolyte composition, and electrode surface films in the harvested electrode cells are different from those in the 18650-cells. In spite of these differences, however, distinct trends were observed in the harvested electrode cell data, which we have used to draw general conclusions about electrode behavior during aging of the 18650-cells.

3. Results and discussion

3.1. Representative data from the 18650-cells

3.1.1. Discharge capacity measurements

Representative C_1/1 and C_1/25 capacity and capacity-fade data from a Gen2 cell that was aged for 88 weeks at 45 °C are shown in Fig. 1. At the start of aging (t = 0 week), the C_1/25 discharge capacity was greater than the C_1/1 discharge capacity, indicating that lithium extraction from the anode and intercalation into the cathode was easier at the slower rate. At this time,

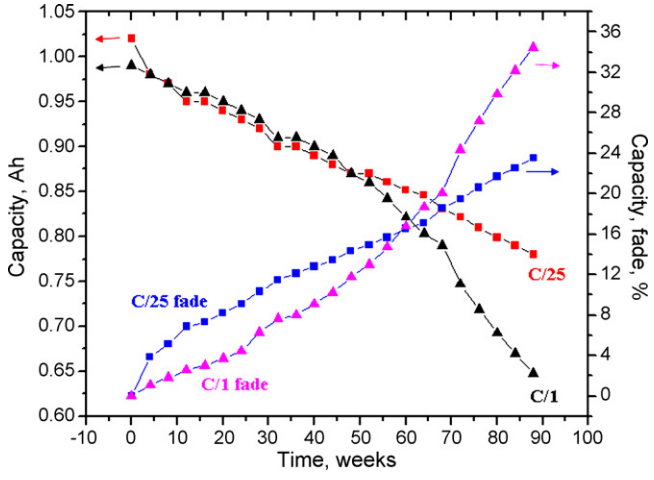

Fig. 1. Representative C_1/1 and C_1/25 capacity and capacity-fade data obtained at 25 °C from an 18650-cell that was calendar-life aged at 45 °C and 60% SOC (3.72 V) for 88 weeks.

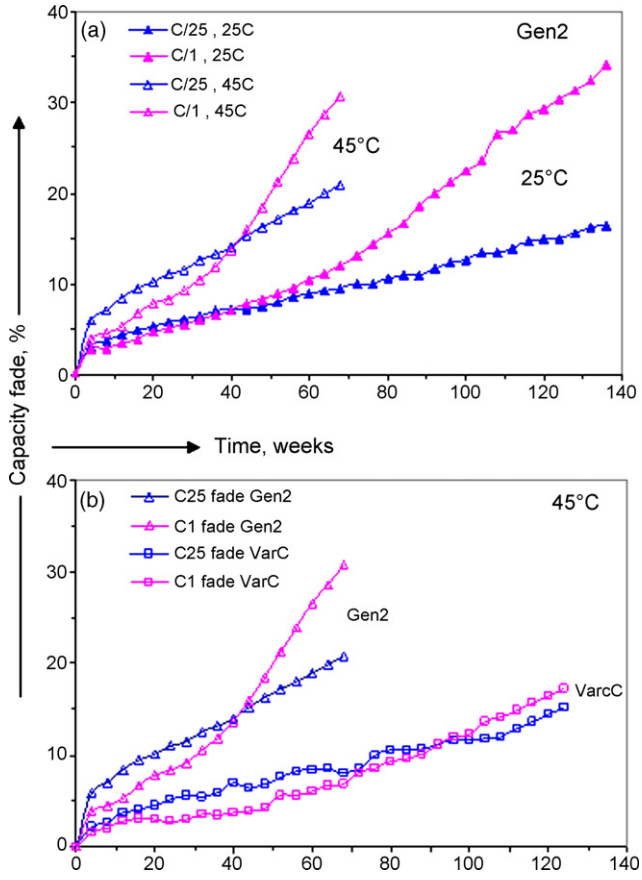

Fig. 2. Representative C_1/1 and C_1/25 capacity-fade data obtained at 25 °C from cycle-life-aged 18650-cells, showing difference (a) between Gen2 cells aged at 25 and 45 °C and (b) between Gen2 and VarC cells aged at 45 °C.

the anode had a well-formed SEI layer because of the formation cycling and the initial characterization measurements. In the early weeks of aging, the C_1/25 capacity decreased faster than the C_1/1 capacity (i.e., the C_1/25 fade rate was greater than the C_1/1 fade rate), so that by t = 4 weeks the C_1/25 capacity was roughly equal to the C_1/1 capacity. The C_1/25 capacity remained roughly equal to the C_1/1 capacity for about 44 weeks at 45 °C. The C_1/1 capacity displayed a more rapid decline after this period. Similar trends were observed for cells tested at 25 °C and at 55 °C.

In general, for all cells tested, the C_1/25 fade rate was greater than the C_1/1 fade rate during the early weeks of aging (<8 weeks). In addition, the cell capacity decrease showed strong dependence on the aging temperature. In Fig. 2a, for example, the C_1/25 capacity decrease for cells aged at 45 °C was greater than for cells aged at 25 °C, especially during the early weeks of aging. The decrease in C_1/1 capacity was more rapid during the later stages and was accelerated by higher aging temperatures. In Fig. 2a, the 45 and 25 °C cells show this behavior after ~28 weeks and ~52 weeks of aging, respectively. Furthermore, at the same aging temperature, the rapid C_1/1 capacity decline occurred earlier for cycle-life cells than for calendar-life cells.

The positive electrode oxide composition also affected cell capacity loss. Fig. 2b compares the C_1/1 and C_1/25 capacity fades of VarC and Gen2 cells that were cycle-life aged at 45 °C.

The capacity fade of the VarC cell was less than that of the Gen2 cell. The VarC cell also showed the rapid C_1/1 decline, but at a lower rate and at a later time than the Gen2 cells. In Fig. 2b, the rapid C_1/1 capacity decline occurred after ~68 weeks and ~28 weeks of aging for the VarC and Gen2 cells, respectively. Because the only known difference between the VarC and Gen2 cells is the oxide composition, the data indicate that the additional Al in the VarC oxide delays the rapid C_1/1 decline during cell aging.

3.1.2. HPPC impedance measurements

Representative area-specific impedance (ASI) data obtained from an 18650-cell by the HPPC test are shown in Fig. 3. Each curve shows impedance data measured at room temperature after aging for the indicated period at 45 °C. Each data marker shows the discharge resistance observed during that pulse plotted against the open-circuit voltage of the cell just before the pulse began. Between each pulse, the cell was discharged until 10% of the initial C_1/1 capacity was extracted, and it was then allowed to equilibrate.

Ideally, the data markers from successive HPPC tests would lie above each other because the open-circuit voltage of the cell would always be the same after removal of the same amount of charge, but as the cells age the data markers move to the left because of a loss in discharge capacity and move upward because of increases in cell impedance. The sharp impedance rise observed at lower cell voltages (<3.55 V) resulted from a decrease in discharge capacity with aging that caused the cell to approach its voltage "knee" ever earlier during the 10% capacity extraction between successive pulses. Pulsing at this voltage knee causes a significant voltage drop that translates into high resistance. However, in the voltage range of interest, which is typically between 3.65 and 3.9 V (Fig. 3 inset), the impedance increases are not affected significantly by cell capacity fade.

Like the capacity data, the ASI increase also depends upon the aging temperature, aging protocol, and oxide composition. Fig. 4 shows the 18 s discharge ASI increase, calculated at 60% SOC, as a function of time for representative Gen2 and VarC

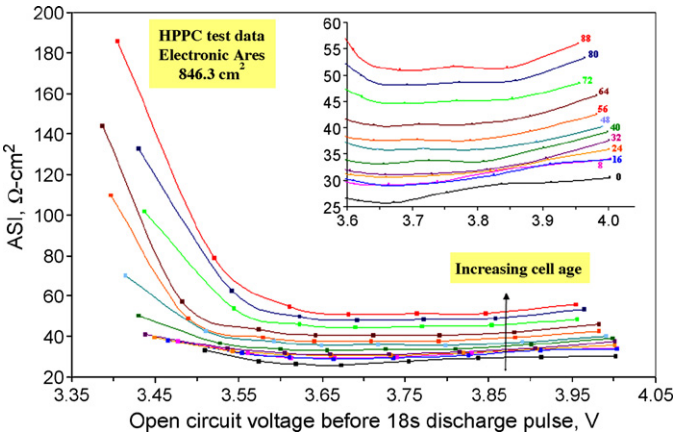

Fig. 3. Representative ASI values measured at 25 °C as a function of OCV from an 18650-cell that was calendar-life-aged at 45 °C and 60% SOC (3.72 V) for 88 weeks—same cell as Fig. 1. The inset is an expanded view; weeks at 45 °C are shown.

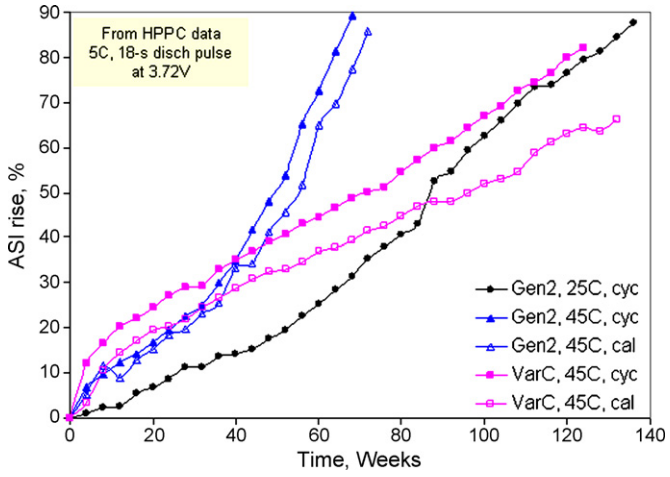

Fig. 4. Area-specific impedance (ASI) rise calculated at 25 °C for Gen2 and VarC cells aged at 25 and 45 °C under calendar-life (cal) and cycle-life (cyc) aging conditions.

cells. It is evident that the rate of impedance rise was relatively rapid in the first 4–8 weeks of aging (region 1), slower during an intermediate aging period (region 2), and relatively rapid again at longer aging periods (region 3).

For Gen2, the rate of ASI increase for the 45 °C cells exceeded the rate of ASI increase for the 25 °C cells. In addition, the ASI increase for the 45 °C cycle-life cells was greater than that of the 45 °C calendar life cells; this aging protocol difference became apparent only after about 28 weeks of aging. The VarC cells showed a faster impedance rise than the Gen2 cells during the first 4 weeks of aging; after this period, the rate of impedance rise of the VarC cells slowed down. Furthermore, the impedance rise for the VarC cycle-life cells was greater than that for the corresponding calendar-life cells.

The Gen2 cells showed relatively rapid impedance rise during the later periods of aging; this behavior was also present, though not as marked, for the VarC cells. The onset of this rapid impedance rise corresponded roughly to the onset of the rapid C_1/1 decline observed in the capacity data. As observed for the capacity data, this onset showed a dependence on aging temperature, aging protocol, and oxide composition. For example, in Fig. 4, the cycle-life Gen2 cells aged at 45 °C and 25 °C showed the rapid impedance rise after ~32 weeks and ~48 weeks of aging; the calendar life Gen2 cells aged at 45 °C showed this onset after ~36 weeks. The onset was significantly delayed (and rather subtle) for the VarC cells; the rate of impedance rise in region 3 was also much lower than that for the Gen2 cells. For example, the VarC cycle-life and calendar-life cells reached the onset of region 3 impedance rise only after ~72 and ~92 weeks at 45 °C, respectively. The data imply that the additional Al in the VarC oxide retards the onset of region 3 impedance rise.

3.1.3. EIS measurements

Representative EIS data over the 10 kHz–0.01 Hz frequency range, obtained at a cell voltage of 3.72 V, are shown in Fig. 5. Each curve shows impedance data measured at 25 °C after the cell was aged at 45 °C for the indicated period. At each measurement, the data show a high-frequency tail (>1 kHz), a

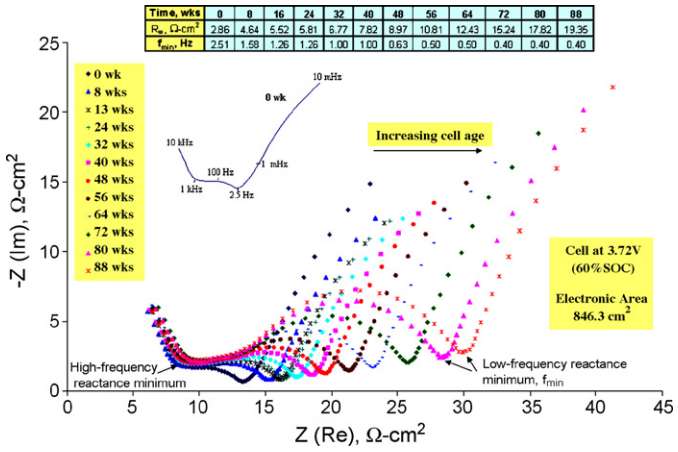

Fig. 5. EIS data (10 KHz–0.01 Hz) at 25 °C on a Gen2 18650-cell—same cell as in Figs. 1 and 3. The inset table shows the mid-frequency arc width (R_w) and frequencies (Hz) at the low-frequency minima (see example arrows in plot) as a function of cell age. The inset figure shows frequency locations for the 0 week data.

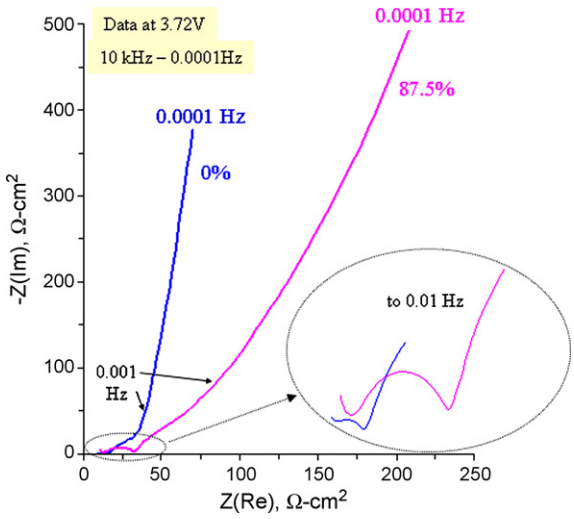

Fig. 7. EIS data (10 KHz–0.0001 Hz) at 25 °C and 3.72 V from two Gen2 18650-cells that showed 0 and 87.5% ASI increase. The inset shows data to 0.01 Hz.

depressed semi-circular arc at mid-frequencies (to ~1 Hz), and a low-frequency (<1 Hz) Warburg tail. These features are readily apparent in the inset figure, which shows only the 0 week data. The high-frequency tail is probably an artifact arising from interaction of the impedance analyzer with the low-impedance cell. The mid-frequency arc is typically associated with interfacial impedance resulting from charge-transfer reactions proceeding simultaneously on both electrodes, while the low-frequency tail is typically associated with diffusional impedance.

On aging, the high-frequency reactance minimum did not change appreciably, but the low-frequency reactance minimum did so. The frequencies at the low-frequency reactance minimum (f_{min}) decreased from 2.5 Hz for the 0-week aged cell to 0.4 Hz for the 88-week aged cell, which suggests that the cell processes slow down with aging. In addition, the mid-frequency arc width (R_w), the portion along the real axis between the high-frequency and low-frequency reactance minima, increased with aging, signifying an increase in the interfacial impedance of the cell. This behavior is illustrated in Fig. 6, where R_w, normalized to the 0 week data, is plotted as a function of cell age. The plot shows features similar to those observed in the ASI increase curve of Fig. 4. The rapid initial impedance increase in region 1 is followed by a slower rise in region 2, which is followed by an accelerating impedance trend in region 3.

Very low-frequency (to 0.0001 Hz) AC impedance data obtained on 18650-cells also provided useful information, especially for cells that were aged for longer periods. Fig. 7 compares data from two Gen2 cells that showed 0% (not aged) and 87.5% (late-life) ASI increase. The Warburg tail of the higher-impedance cell displayed a significantly higher resistance at very low frequencies, which indicates that diffusion phenomena play an important role in the impedance increases observed after long-term cell aging (e.g., as in region 3).

Testing temperature had a significant effect on cell impedance. Fig. 8 shows EIS data, obtained at 25 and 45 °C, on a highly aged cell. The cell impedance was significantly lower at the higher test temperature. In addition, R_w was much smaller at 45 °C, which indicates that the physical features that produce

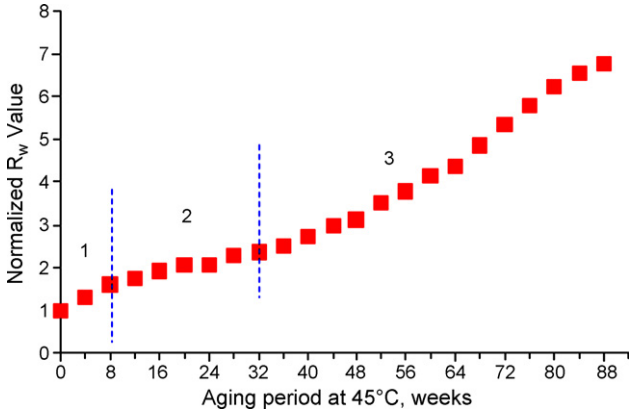

Fig. 6. The mid-frequency arc width (R_w) plotted as a function of cell age for EIS plots in Fig. 5; the R_w values are normalized to those at the beginning of the aging period (0 week).

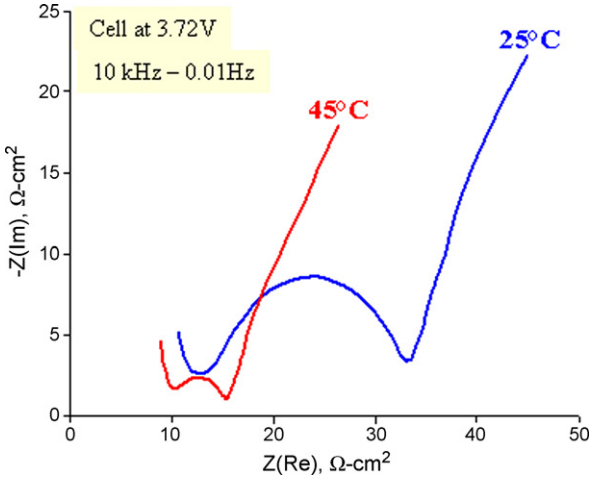

Fig. 8. Effect of test temperature on EIS data (10 KHz–0.01 Hz) obtained at 3.72 V on a Gen2 18650-cell that showed 87.5% ASI increase—same cell as in Fig. 7.

the mid-frequency arc are very temperature-sensitive. Changing the test temperature by even a few degrees had a profound effect on R_w. Our data also showed that the Warburg tail length was unaffected by temperature changes in the 25–55 °C range: the physical processes that produce the diffusion tail are not temperature-sensitive in this range.

Although the HPPC and EIS information from 18650-cells are very valuable, the data cannot identify the electrodes or mechanisms that produce the changes in impedance with aging. That information can only be obtained from data on electrodes harvested from the aged cells, described in Section 3.2.

3.2. Representative data from harvested electrodes

3.2.1. Positive electrode capacity measurements

Representative charge–discharge data (versus Li metal) obtained with a 0.064 mA current for positive electrodes harvested from Gen2 and VarC cells that displayed various levels of capacity fade are shown in Fig. 9. The coin cell capacities were lower for electrodes harvested from 18650-cells that showed greater capacity loss. In Fig. 9a, for example, positive electrodes harvested from calendar-life aged Gen2 cells showing 0, 3.7, 14, 18.3, and 34.4% capacity fade have capacities of 2.56, 2.36, 2.3, 2.03, and 1.8 mAh, respectively. Similar trends were observed for electrodes harvested from the 25 and 45 °C cycle-life aged cells. The harvested electrode capacities were consistent with the capacity fade displayed by the parent cell. Because the counter electrode is an infinite source of lithium, the coin cell capacity variations indicate changes in the positive electrode during accelerated aging of the 18650-cells.

In addition to capacity loss, cycling hysteresis becomes more prominent with electrode age. Electrodes from early-life (region 1) and mid-life (region 2) cells showed little hysteresis, whereas late-life electrodes (region 3) showed significant hysteresis. Such hysteresis results from the inability of the electrode to attain thermodynamic equilibrium during the constant current cycling. The increasing cycling hysteresis indicates that, as the cell ages, the positive electrode becomes unable to deliver or accept lithium at rates that were previously possible.

Cycling rate had a significant effect on the measured cell capacities. Electrodes from early- and mid-life cells showed significant capacity gains and improved cycling hysteresis at lower currents so their capacities often equaled that of the 0% capacity fade (CF) electrode. For example, in Fig. 10a, the electrode capacities are 2.28, 2.34, and 2.36 mAh when cycled with 0.064, 0.032, and 0.008 mA current, respectively. Significant capacity gains and cycling hysteresis improvements were also observed at lower currents for electrodes from highly aged cells. For example, in Fig. 10b, the electrode capacities are 1.77, 1.91, and 2.05 mAh when cycled with 0.064, 0.032, and 0.008 mA current, respectively. For these electrodes, however, the capacity values were significantly lower than for the 0% CF electrode (2.56 mAh), and cycling hysteresis was evident in the data even at the low currents used in our measurements.

Cycling the VarC positive electrode at lower current also resulted in capacity gain and improvements in cycling hysteresis. When cycled with a 0.008 mA current, a positive electrode from a 2.7% CF cell (Fig. 10c) showed a capacity comparable with that of the 0% CF VarC electrode. The increased capacities at slower cycling rates indicate that electrode capacity loss is a manifestation of impedance rise (i.e., the particles are not electronically isolated).

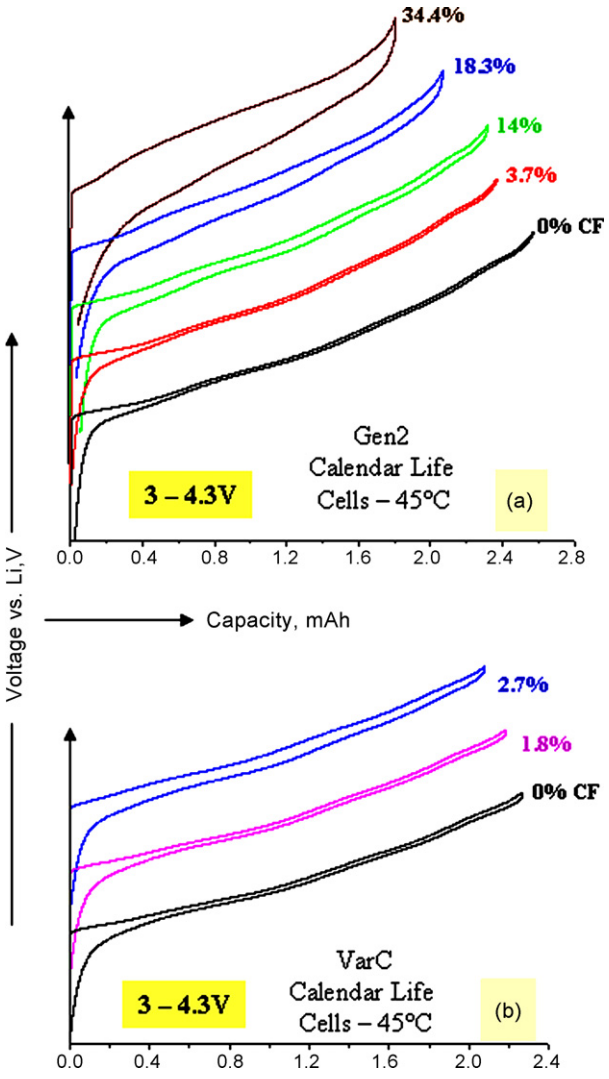

Fig. 9. Charge–discharge cycles (vs. Li) for positive electrodes harvested from (a) Gen2 and (b) VarC cells. Data were obtained in coin cells at 25 °C, with a 0.064 mA cycling current, in the 3–4.3 V range. Capacity fade (CF) of the 18650-cells is shown in the figures. Curves have been offset vertically for clarity.

In an attempt to restore their "original" capacity, positive electrodes harvested from aged cells were rinsed in various solvents and dried thoroughly before coin cell assembly. As expected, rinsing the 0% CF electrodes in dimethyl carbonate (DMC), EC:EMC (3:7 by wt.), and H_2O did not alter sample cycling performance. However, DMC- and EMC-rinsing of positive electrode materials from mid- and late-life cells degraded sample cycling performance. Fig. 11a shows data on electrodes from a 34.4% CF cell. The DMC-rinsed samples had lower capacities and showed greater polarization on both charge and discharge, whereas H_2O-rinsing and EC:EMC-rinsing did not alter electrode cycling performance. Because our rinse protocol was far

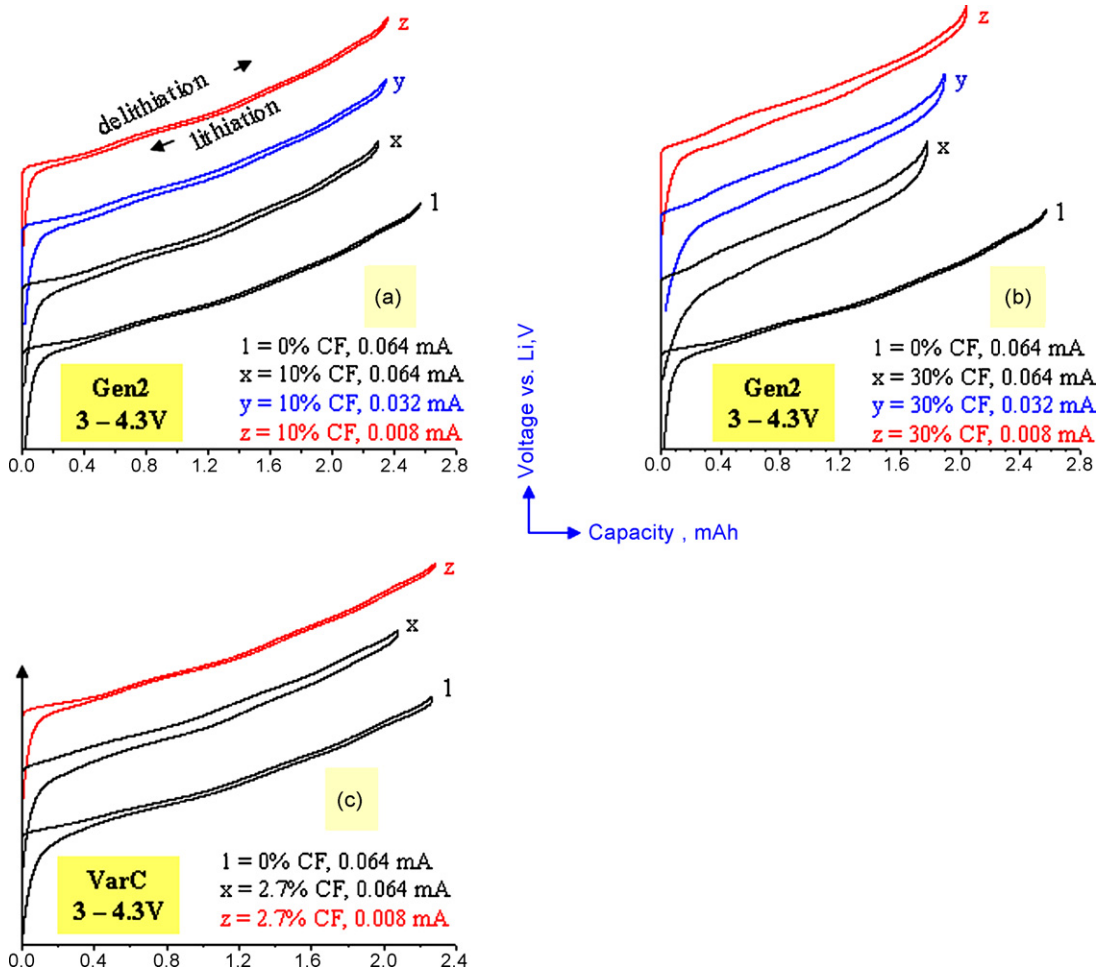

Fig. 10. Cycling-rate effect on measured capacity at 25 °C for positive electrodes harvested from 18650-cells: (a) Gen2, 10% CF; (b) Gen2, 30% CF; (c) VarC, 2.7% CF. Curves have been vertically offset for clarity. Data from 0% CF cells are shown for comparison.

too gentle to produce oxide particle damage, the data suggest that electrode capacity can be altered by factors that are strictly external to the oxide crystals. Furthermore, our data suggest that electrode performance degradation is affected by the rinse solvent polarity: the more non-polar the rinse solvent, the greater is the electrode degradation.

In another attempt to restore "original" capacity, positive electrodes harvested from aged cells were cycled at 45 and 55 °C because higher cycling temperatures are known to speed up the electrochemical kinetics. At these higher temperatures, electrodes from mid-life cells showed capacities that were comparable to those of the starting electrodes. Therefore, the capacity loss displayed by the electrodes at room temperature was mostly a manifestation of impedance rise that reduced electrode rate capability. Electrodes from late-life cells showed higher capacities and reduced cycling hysteresis at 55 °C than they did at 25 °C (Fig. 11b). However, the cycling hysteresis indicated that the cycling was not under equilibrium conditions, even at this higher temperature. That is, for the late-life cells, a significant portion of the apparent 25 °C capacity fade arises from the electrode impedance; a small portion of the capacity loss may be from inaccessible charge storage, which could result from electronically isolated particles.

3.2.2. *Negative electrode capacity measurements*

Representative charge–discharge data (versus Li metal) obtained with a 0.064 mA current for the negative electrodes are shown in Fig. 12. All curves displayed the staging effects expected during lithium intercalation–deintercalation into graphite materials. In general, the negative electrode capacities were lower with increasing cell age; that is, a portion of the capacity loss displayed by the aged 18650-cells can be attributed to the negative electrode. In Fig. 12a, the negative electrodes from 18650-cells showing 0, 3.7, 18.3, and 34.4% capacity fade had capacities of 2.94, 2.82, 2.68, and 2.30 mAh, respectively; the corresponding positive electrodes had capacities of 2.56, 2.36, 2.03, and 1.8 mAh, respectively. That is, in spite of the capacity loss, the graphite electrode (even from highly aged cells) had sufficient capacity to accept lithium-ions from the positive electrode. These data imply that metallic lithium deposition on the negative electrode during cell charging was unlikely even for late-life 18650-cells.

For the negative electrodes, cycling hysteresis was observed even for samples that were not aged. The hysteresis behavior of the various samples was quite similar, with the exception of highly aged electrodes. In addition, the capacity gain from slower-rate cycling was very small (Fig. 13a). These capacity

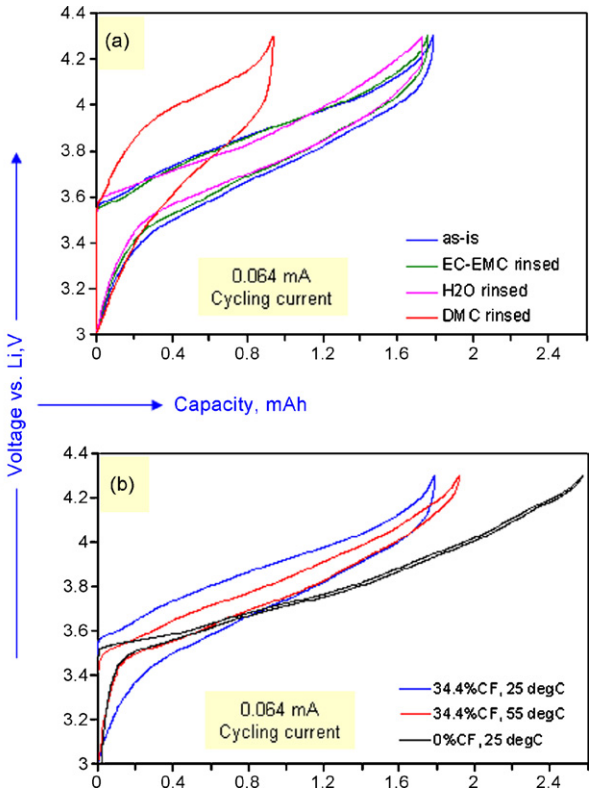

Fig. 11. Capacity data (vs. Li) at 25 °C for positive electrodes extracted from a 34.4% CF Gen2 cell, showing (a) effect of electrode rinsing and (b) effect of test temperature. In (b), the 0% CF electrode data are shown for comparison.

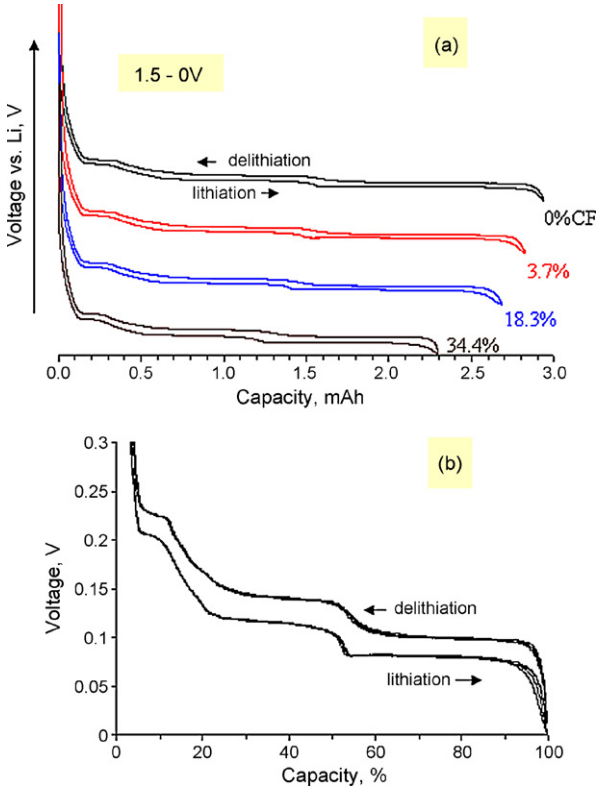

Fig. 12. (a) Cycling data at 25 °C from harvested anodes (vs. Li metal) obtained with a 0.064 mA current in the 1.5–0 V range; capacity fade of the 18650-cells is shown in the figure. Curves have been offset for clarity. (b) Same data as in (a), but in the 0.3–0 V range after cell capacity variations are normalized out.

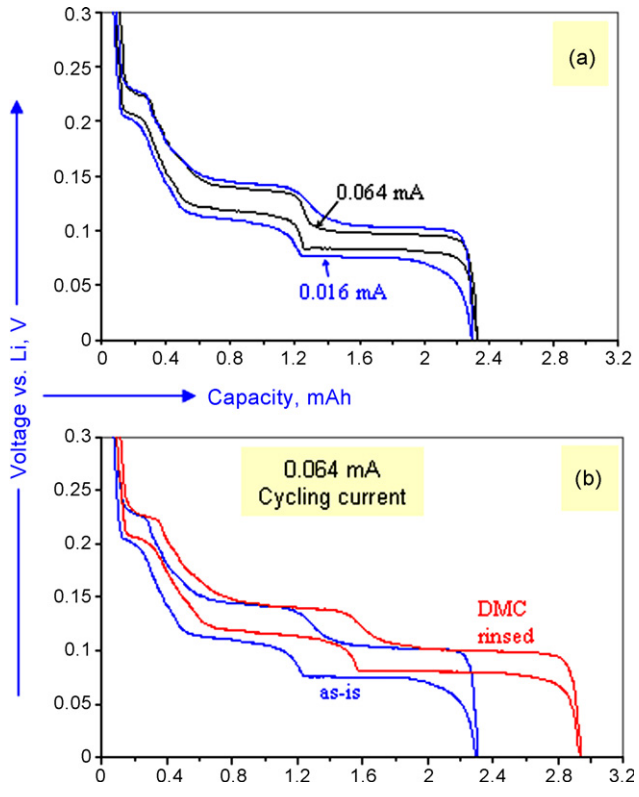

Fig. 13. Effect of (a) cycling rate and (b) DMC rinsing on negative electrodes harvested from a Gen2 cell that showed 34.4% capacity fade. In (a) the cycling currents are 0.064 and 0.016 mA; in (b) the cycling current is 0.064 mA.

data also suggest that the negative electrode impedance change with aging is small.

The cycling data clearly show that the negative electrode suffers a capacity loss during aging of the 18650-cells. However, this capacity loss does not seem to be from damage to the graphite particles. This is evident in Fig. 12b, which shows cycling data after the cell capacity variations have been normalized. The similarity of the various curves indicates that the graphite particles that contribute to electrode capacity behave very similarly. This is also evident from capacity measurements conducted on negative electrode samples that were rinsed in DMC solution prior to cycling (versus Li metal). Rinsed samples, even from late-life cells, showed capacities that were comparable to those of electrodes that were not aged (Fig. 13b), indicating that the graphite structure was unchanged. The similarity between the rinsed electrode and fresh electrode capacities also implies that there is no loss of active material into the electrolyte solution. Therefore, the capacity loss displayed by the aged negative electrodes must result from isolation of some graphite particles by electronically insulating portions of the SEI, which are washed away during the DMC-rinse [13].

3.2.3. Impedance measurements

EIS data (10 kHz–0.01 Hz) at 25 °C for the full cell, and positive and negative electrodes, obtained from a reference electrode cell containing electrode materials harvested from Gen2 and VarC cells are shown in Fig. 14; the measurements were conducted at a full-cell voltage of 3.72 V. The consistency of the

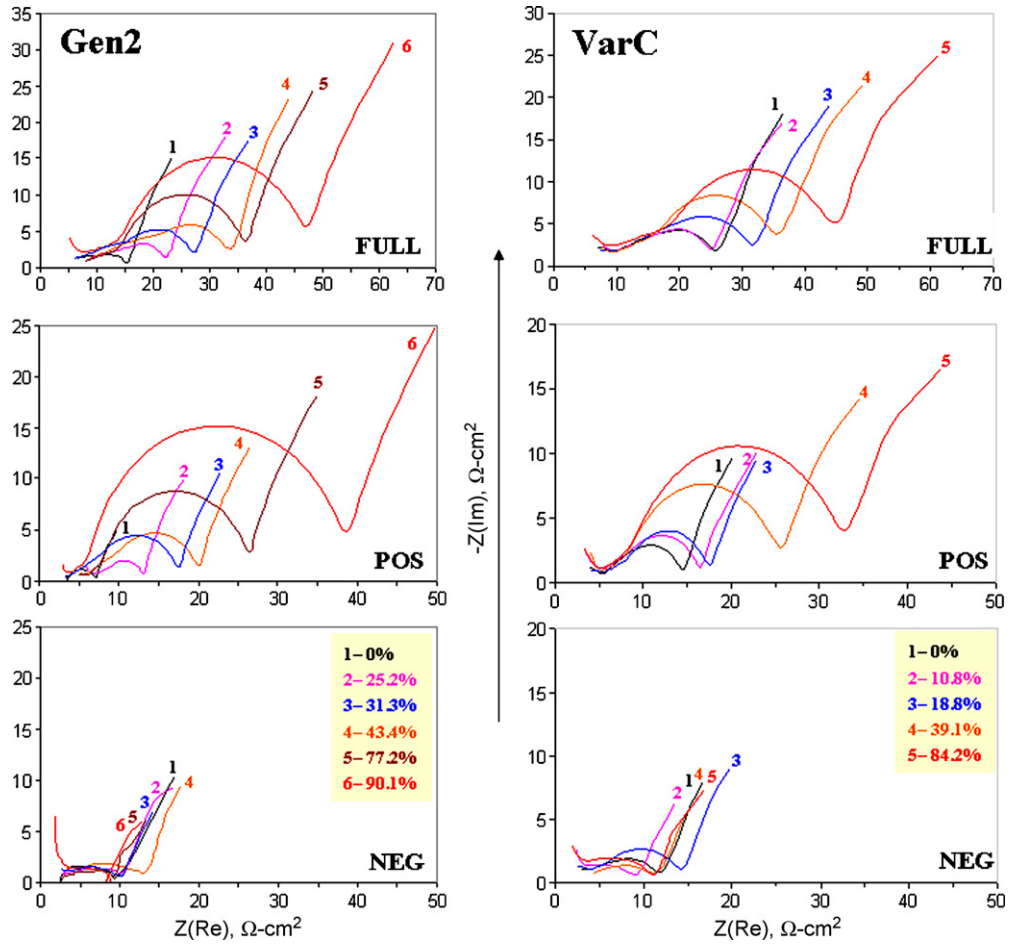

Fig. 14. EIS data (10 kHz–0.01 Hz) at 25 °C for the full cell, and positive and negative electrodes, harvested from Gen2 and VarC cells; the impedance rise of the 18650-cells is indicated in the figures.

impedance data was confirmed by matching the full-cell data with the sum of the positive and negative electrode data from the reference electrode cells. In general, full-cell impedance increase trends were consistent with the impedance changes displayed by the corresponding 18650-cells.

It is evident from Fig. 14 that the positive electrode was the main contributor to the full-cell impedance for both the Gen2 and VarC cells. In addition, the main increase in the positive electrode impedance is in the mid-frequency semicircular arc, which suggests that the charge-transfer and mass-transfer characteristics at the positive electrode–electrolyte interface degrade with aging. The negative electrode impedance data were all similar within the range of experimental uncertainty. The EIS data trends were consistent with the ASI data trends (not shown) determined by the HPPC test on harvested electrode materials.

To shed further light on the impedance increase, EIS data to low frequencies (0.00025 Hz) were obtained on the harvested electrodes. Fig. 15 shows low-frequency data obtained on electrodes from an 18650-cell that was not aged (0% fade). At frequencies below 1 mHz, the positive electrode impedance curve is almost parallel to the *Y*-axis, indicating that the processes below 1 mHz, such as the charge-transfer processes that occur within the oxide particles, are purely capacitive in nature. The negative electrode data also show an increase in the capacitive component at frequencies below 1 mHz, but with an accompanying increase of the resistive component; the data indicates that the distribution of characteristic diffusion lengths is greater for the negative electrode.

The low-frequency data obtained on harvested negative electrodes from aged cells were very similar to those shown in Fig. 15 (i.e., the impedance curve was little changed by electrode aging). However, important changes were observed in the positive electrode data, as shown in Fig. 16. For example, the late-life electrode (90.1% ASI rise) data show a significant resistive component at very low frequencies. Because the low-frequency portion is an extension of the Warburg tail that is typical of diffusion-related processes, the impedance increase indicates an increased difficulty of lithium transport into and through the oxide particles (i.e., a “slowing” of the oxide particles with increasing cell age). This slowing of the oxide particles was also apparent in the harvested electrode capacity data, as described previously (Section 3.2.1). The resistive component is also present, but is not as dominant, in the mid-life cell electrode (31.3% ASI rise) data, which show a mostly capacitive tail at very low frequencies. Because the differences in the negative electrode response at low frequencies are insignificant compared to those of the positive electrode, it is clear that the significantly higher resistance displayed by aged cells during EIS testing at

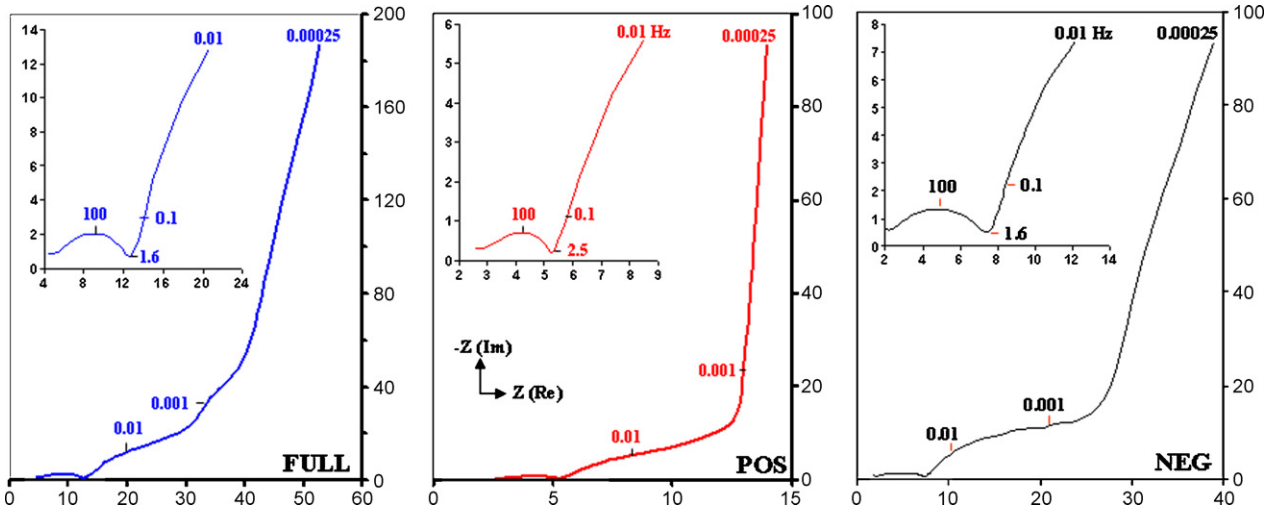

Fig. 15. Typical EIS data (10 kHz–0.000250 Hz) at 25 °C for the full cell, and positive and negative electrodes, obtained from a reference electrode cell containing electrode materials from a Gen2 18650-cell that was not aged. The inset is an expanded view of data in the 10 kHz–0.01 Hz range. Frequency (Hz) information is shown in the figures. The *X*- and *Y*-axes show the real and imaginary values of the ASI ($\Omega\,cm^2$), respectively.

low frequencies (Fig. 7) is associated with diffusion phenomena in the positive electrode.

Testing temperature had a significant effect on the EIS data. Increasing the test temperature lowered the cell impedance by reducing the impedance at both the positive and negative electrodes. The reduction in the positive electrode mid-frequency arc width (R_w) with test temperature (Fig. 17) indicates that the electrode–electrolyte interfacial features responsible for R_w are

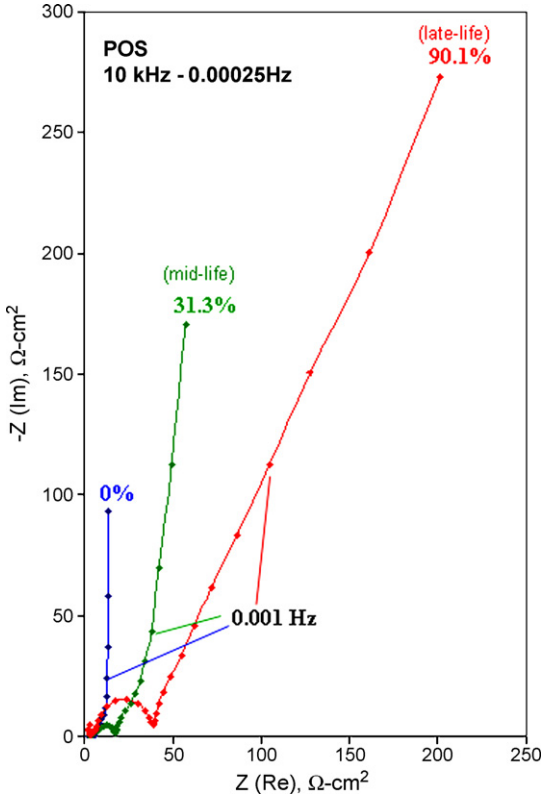

Fig. 16. EIS data at 25 °C obtained on positive electrodes harvested from Gen2 cells; impedance rise of the 18650-cells is shown in the figure.

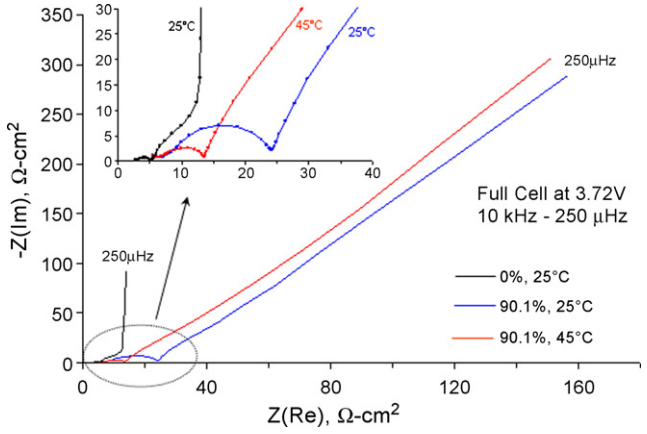

Fig. 17. Effect of test temperature on positive electrode impedance. The 25 and 45 °C data are for an electrode harvested from a Gen2 cell that showed 90.1% ASI rise; 25 °C data from a 0% PF cell are shown for comparison. Inset shows an expanded view of the high-frequency region.

responsive to testing temperature: the higher the test temperature, the less is the effect of this interfacial feature. The Warburg impedance tail, on the other hand, is not significantly changed by testing at different temperatures (20–55 °C). The physical processes responsible for the positive electrode diffusion tail are not sensitive to temperature in this narrow range. The increases in the mid-frequency arc width and Warburg-tail length appear to be the result of two distinct and perhaps independent mechanisms that become prominent in different stages of the cell's life. These will be correlated to physicochemical changes in the positive electrode and described in a separate article.

4. Summary and conclusions

High-power 18650-type lithium-ion cells containing $LiNi_{0.8}Co_{0.15}Al_{0.05}O_2$- or $LiNi_{0.8}Co_{0.1}Al_{0.1}O_2$-based positive electrode, Mag-10 negative electrode, and a $LiPF_6$-bearing EC:EMC electrolyte show impedance rise and capacity loss

with accelerated aging. Electrochemical studies conducted on electrodes harvested from these cells lead to the following conclusions:

(1) The positive electrode is mainly responsible for cell impedance rise; the negative electrode's contribution is small.
(2) The impedance rise of the positive electrode manifests itself in (a) increasing width of the mid-frequency arc and (b) increasing the Warburg-tail length. The physical features that produce the positive electrode mid-frequency arc are affected by the EIS test temperature. The Warburg tail, on the other hand, appears to be independent of temperature in the 20–55 °C range.
(3) The C_1/1 capacity reduction with aging results from factors that include the following: (a) side reactions that consume lithium at the negative electrode and (b) an impedance rise that reduces the ability of the positive electrode to deliver and accept lithium.
(4) The capacity of aged negative electrodes can be restored by DMC rinsing, which indicates that the capacity loss results from pore-clogging or isolation of graphite particles by electronically insulating surface films.
(5) The capacity of aged positive electrodes from region 2 cells can be restored by increasing cell test temperature, which reduces electrode impedance, whereas the capacity of aged electrodes from region 3 cells cannot be restored by increasing temperature or by gentle rinsing in DMC.

Acknowledgments

The submitted manuscript has been created by UChicago Argonne, LLC, Operator of Argonne National Laboratory ("Argonne"). Argonne, a U.S. Department of Energy Office of Science Laboratory, is operated under Contract No. DE-AC02-06CH11357. The U.S. Government retains for itself, and others acting on its behalf, a paid-up nonexclusive, irrevocable worldwide license in said article to reproduce, prepare derivative works, distribute copies to the public, and perform publicly and display publicly, by or on behalf of the Government.

We are grateful for the help of A. Jansen, S. Jones, and G. Henriksen at Argonne National Laboratory; C. Ho, C. Motloch, and K. Gering at Idaho National Laboratory; and E. Sammann at the Center for Microanalysis of Materials, University of Illinois at Urbana-Champaign.

References

[1] M. Anderman, J. Power Sources 127 (2004) 2.
[2] S.S. Zhang, J. Power Sources 161 (2006) 1385.
[3] R.G. Jungst, G. Nagasubramanian, H.L. Case, B.Y. Liaw, A. Urbina, T.L. Paez, D.H. Doughty, J. Power Sources 119 (2003) 870.
[4] J. Fan, J. Power Sources 117 (2003) 170.
[5] J.P. Fellner, G.J. Loeber, S.S. Sandhu, J. Power Sources 81 (1999) 867.
[6] D. Aurbach, B. Markovsky, A. Rodkin, M. Cojocaru, E. Levi, H.J. Kim, Electrochim. Acta 47 (2002) 1899.
[7] I. Bloom, S.A. Jones, V.S. Battaglia, G.L. Henriksen, J.P. Christophersen, R.B. Wright, C.D. Ho, J. Belt, C.G. Motloch, J. Power Sources 124 (2003) 538.
[8] I. Bloom, B.G. Potter, C.S. Johnson, K.L. Gering, J. Power Sources 155 (2006) 415.
[9] J.P. Christophersen, C.D. Ho, C.G. Motloch, H.L. Hess, J. Electrochem. Soc. 153 (2006) A1406.
[10] I. Bloom, B.W. Cole, J.J. Sohn, S.A. Jones, E.G. Polzin, V.S. Battaglia, G.L. Henriksen, C. Motloch, R. Richardson, J. Power Sources 101 (2001) 238.
[11] PNGV Battery Test Manual, Revision 3, INEEL, February 2001.
[12] D.P. Abraham, S.D. Poppen, A.N. Jansen, J. Liu, D.W. Dees, Electrochim. Acta 49 (2004) 4763.
[13] M. Herstedt, D.P. Abraham, J.B. Kerr, K. Edstrom, Electrochim. Acta 49 (2004) 5097.